JOURNAL OF APPLIED ELECTROCHEMISTRY 25 (1995) 716–728

Effect of state of charge on impedance spectrum of sealed cells
Part I: Ni–Cd cells

V. V. VISWANATHAN,*‡ A. J. SALKIND,‡§ J. J. KELLEY, ‡§ J. B. OCKERMAN §

Department of Chemical Engineering, Rutgers University, Piscataway, NJ, 08855, USA‡ and UMDNJ-Robert Wood Johnson Medical School, Bioengineering Section, 675 Hoes Lane, Piscataway, NJ, 08854, USA§

Received 7 February 1994; revised 20 October 1994

Alternating current impedance spectroscopy (ACIS) was performed on commercial sealed Ni–Cd cells. A method previously developed in the literature was modified to determine the state of charge of sealed Ni–Cd cells by obtaining the impedance spectrum in a wide frequency range. The impedance parameters were sensitive to state of charge at low frequencies. A modified Randles' circuit was used to fit the impedance data. Appropriate modifications were made to account for an additional high frequency arc or a low frequency finite diffusion element. The effect of the state of charge on the equivalent circuit parameters was determined.

List of symbols

R_Ω ohmic resistance of battery (ohms)
C_{dl} double layer capacitance (F)
Q_1 constant phase element representing double layer capacitance
Q_2 constant phase element representing Warburg diffusion
O finite diffusion element
R_t charge transfer resistance (Ω)
R_s, R_p equivalent series and parallel resistance (Ω)
C_s, C_p equivalent series and parallel capacitance (F)

1. Introduction

Several investigators have studied the effect of the state of charge and state of health on the impedance parameters of Ni–Cd cells [1–6]. Barton *et al.* [2] studied the effect of state of charge on the impedance of a sintered nickel hydroxide electrode. The charge transfer resistance R_t decreased with increase in state of charge, while the double layer capacitance C_{dl} increased with increase in charge state. The product of R_t and C_{dl} increased exponentially with increase in state of charge. Suresh and Sathyanarayana [3] measured the impedance of sealed Ni–Cd cells at low states of charge by potentiostatting the cells in the voltage range 0 to 1.3 V. They found that at such low charge states, the impedance of the nickel electrode dominated the cell impedance. The cell impedance exhibited capacitive behaviour between 0.3 to 0.8 V, while the hydrogen evolution reaction (charge transfer) controlled the cell impedance at 0 V. Blanchard [4] determined the effect of state of charge on the R_t, C_{dl}, R_Ω, and low frequency phase angle ϕ. The spectrum was obtained during charge or discharge of the cells. The ohmic resistance was not significantly dependent on the state of charge. The charge transfer resistance R_t increased during charge and discharge. The double layer capacitance increased with increase in state of charge. Haak *et al.* [5] found that a rapidly increasing value of the low frequency slope in the Nyquist plot for a Ni–Cd cell was indicative of potential cell failure. Reid [6] studied the effect of cycle life on the impedance spectrum of aerospace design 'Super Ni–Cd cells'. Various circuits were used to represent the cell impedance. A parallel circuit of charge transfer resistance and constant phase element in series with the ohmic resistance was found to fit the data well. The charge transfer resistance decreased at low states of charge over the first 500 cycles, with no significant changes in other circuit parameters. Although this work did not use the cell case as a reference in order to separate the individual electrode contributions [7], studies being conducted on sealed Ni–H_2 cells were targeted to determine the contribution of the nickel electrode impedance.

Since the double layer capacitance and charge transfer resistance are determined by fitting the data to a predetermined circuit, such an approach may not be very accurate. Since there is no net generation or removal of OH^- ions during the charge/discharge reactions in Ni–Cd cells, the electrolyte does not participate significantly. Hence the ohmic resistance for nickel cadmium batteries is not very sensitive to the state of charge. Determination of the low frequency phase angle can be done either visually or by fitting. In both cases, there is a possibility for error. In the case of nickel cadmium cells, the low frequency data

*Present address: Battelle Memorial Institute, Electrochemical Technology Group, 505 King Avenue, Columbus, Ohio 43201.

0021-891X/93

shows scatter and dual slope [5]. Sathyanarayana and Gopikanth [1] determined the effect of state of charge on phase angle (ϕ), C_s and C_p, where C_s and C_p are the battery equivalent series and parallel capacitance respectively. The study was carried out in the frequency range 5–30 Hz. Since the impedance parameters are most sensitive to state of charge at low frequencies [8], the above parameters were determined at frequencies ranging from 0.01–25 Hz in this work. An attempt has also been made to correlate the equivalent circuit parameters with the state of charge.

2. Experimental procedure

The Ni–Cd cells tested were two Sanyo 2 Ah cells (labelled Ni–Cd cell 1 and cell 3) and two Panasonic 1.8 Ah cells labelled Ni–Cd cell 5 and cell 6). The cells were cycled by charging at the $C/4$ rate for 5 h, resting for 1 h and discharging at the $C/5$ rate using a cutoff voltage of 1 V, where C is the nominal capacity of the cells. Cycling was done using a 'life cycle tester' developed by Propel Inc. After a few cycles, impedance measurements were performed on the batteries at various states of charge (SOC) as described below, with the measurements starting at 0% SOC.

The cells were discharged at $C/5$ rate to 1 V cutoff and impedance measurements were done at 0% SOC after the cells were on open circuit for 8 h. The cells were charged at $C/5$ rate for 1 h and impedance spectrum obtained after 8 h on open circuit. The cells were discharged at $C/5$ rate to 1 V after obtaining the spectrum to determine their actual state of charge. The cells were then charged at $C/5$ rate for 2 h. After 8 h on open circuit, the cell impedance spectrum was obtained. The cells were discharged at $C/5$ rate to 1 V and charged at $C/5$ rate for 3 h. This was repeated till impedance data was obtained at 100% SOC. The internal resistance was measured at each SOC at 1000 Hz using Hewlett–Packard milliohmmeter (model 4328A).

A review of the method of collecting impedance data over a wide frequency is given in EG&G PARC application note AC-1 [9]. The a.c. impedance spectrum was obtained using a potentiostat (PAR model 173) with a plug-in interface (PAR model 276), a lock-in amplifier (LIA, model 5301) and an IBM computer (286 XT). Electrochemical Impedance Systems software (model 388) was used to interface between the computer, the LIA and the potentiostat. The impedance at frequency greater or equal to 5 Hz was measured using sine waves at discrete frequencies. The potentiostat generated the input potential signal (5 mV amplitude) on command from the software. The signal was fed to the LIA and the cell. The current output from the cell was also fed to the LIA. The input potential signal and the current output were split into real and imaginary components by the LIA and fed to the computer. The software computed the impedance. At low frequencies, the fast Fourier technique (FFT) was used to speed up the data acquisition. A mixture of 20 signals, each of a different frequency, was generated by the computer and sent to the cell. (The LIA was bypassed.) The output from the cell was resolved into the individual frequencies and the impedance was computed at each frequency. This technique is twice as accurate as the single sine technique at the same measurement rate or twice as fast for the same accuracy. An additional advantage to this technique is that its root mean square excitation is 35% of the peak amplitude as compared to 70% for a sine wave [10]. Hence, the electrochemical system is subjected to smaller perturbations than application of sine wave at individual frequencies.

3. Equivalent circuit analysis

Various circuits may be proposed to represent the battery impedance and the circuit parameters can be determined by fitting the data to the circuit. The software used in this work for equivalent circuit fitting was developed by Boukamp [11]. Different portions of the data can be fitted either with a line or a circle in the impedance or admittance plane. An arc in the impedance plane represents a resistance in series with a parallel (RQ) circuit, where Q is a constant phase element. The parallel (RQ) circuit can also be analysed in the admittance plane by fitting with a straight line. A line in the impedance plane represents a series RQ circuit. The inductive data was fitted by a parallel (RL) circuit in series with the rest of the circuit. Deletion of the inductive data didn't have any effect on the remaining circuit parameters. Hence, the cell circuit parameters were determined after deleting the inductive points. The cell impedance was represented by a modified Randles' circuit. According to the porous electrode theory, developed by de Levie [12], the overall electrode impedance is proportional to the square root of the product of the axial (inside pores) and interfacial impedance. Hence, one cannot expect to successfully extract the actual double layer capacitance or the Warburg coefficient from the data. Due to this, a constant phase element was used instead of the double layer capacitance and Warburg element.

The admittance of a constant phase element Q is given by $Y(j\omega)^n$, where Y and n are adjustable parameters of the constant phase element (CPE) Q. The value of $n = 1$ corresponds to capacitance ($Y = C$), $n = -1$ corresponds to inductance ($Y = -1/L$) and $n = 0.5$ corresponds to Warburg diffusion. At very low frequencies, the data for certain cells in the Nyquist representation bends over to the real axis. This was modelled by a finite diffusion length element in which the concentration of the diffusing species is fixed at one boundary (surface of the electrode). In such a case, the assumption of infinite pore length fails. The equivalent circuit software models such finite diffusion length data by a cotangent hyperbolic function O, the admittance $Y(\omega)$ of which is given by $Y(\omega) = Y_0(j\omega)^{0.5} \operatorname{Coth}[B(j\omega)^{0.5}]$. Y_0 is the adjustable parameter that contains the diffusion coefficient, and

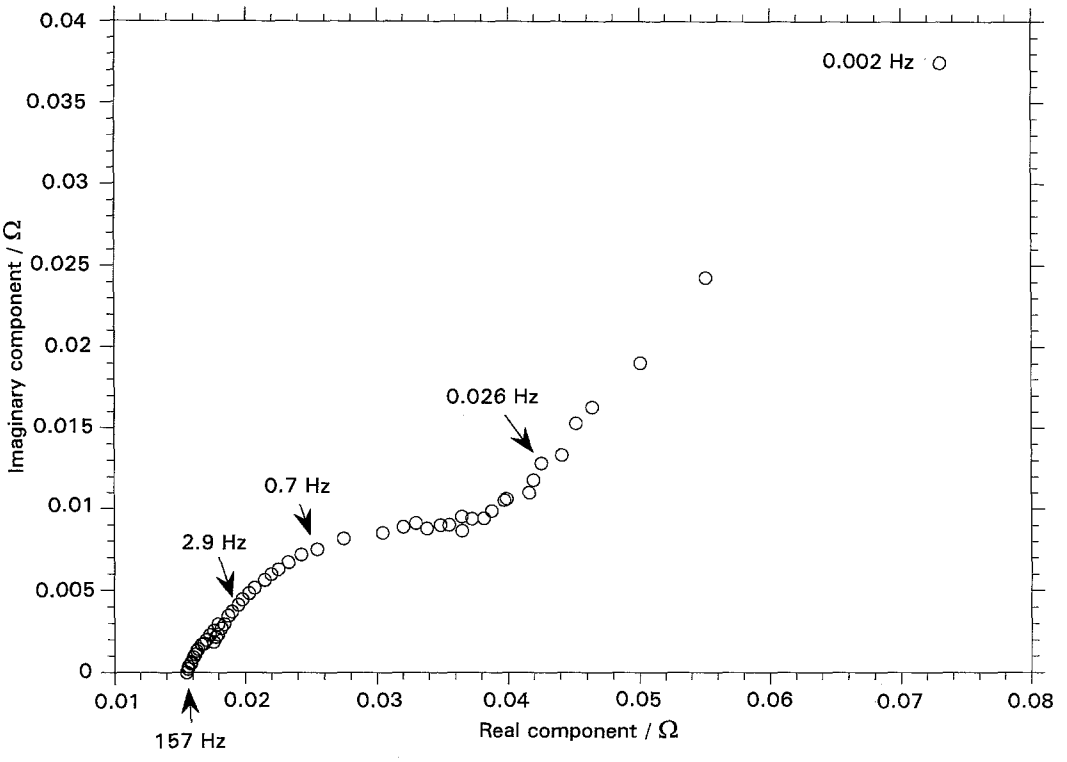

Fig. 1. Nyquist plot for Ni–Cd cell 5 at 20% SOC in the frequency range 0.002–158 Hz.

B takes into account the physical dimensions of the sample.

Fitting was carried out starting at the high frequency end with the data in the impedance form. The inductive portion of the data was deleted prior to fitting. The points at the high frequency end were fitted with an arc by partial non-linear least squares fitting. After subtracting the ohmic resistance, the data was transformed to the admittance plane. After removing the high frequency scatter, the data was fitted with a straight line. The CPE corresponding to the double layer capacitance was subtracted, and the data transformed to the impedance plane. The high frequency scatter was deleted and the remaining points were fitted with a straight line. The series circuit RQ of the charge transfer resistance and CPE corresponding to the Warburg element was subtracted. Uniform scatter around the origin was indicative of the good nature of the fit.

A total nonlinear least squares fit was performed on the data using the subtraction code from the subtraction file. At the end of the fit, the data and simulated results were plotted in the impedance plane, admittance plane and in the Bode format. The relative error in fit for the real and imaginary components were also plotted.

4. Results and discussion

4.1. *Impedance data*

The frequency range for all the states of charge is 0.002–250 Hz. Since the inductive points and extreme scatter in the low frequency region were deleted, the actual lower and upper limits for each cell vary slightly. Figure 1 shows the Nyquist plots for Ni–Cd cell 5 at 20% SOC. A depressed semicircle at high and midfrequency, while at low frequency, diffusive behaviour is observed. In general, the Nyquist plot gave more scatter, which are significantly reduced in the Bode plots.

4.2. *State of charge determination*

Figure 2(a) shows the Bode plot (impedance) for Ni–Cd cell 5 at various states of charge, while Fig. 2(b) shows the corresponding phase angle plot. The impedance at 0% state of charge was high. At high frequencies, the impedance at other states of charge was the same. At low frequencies, the slope, and hence the magnitude of the impedance increased with increase in state of charge in the 20–80% range. Since the magnitude of the impedance at low frequency decreased from 0% to 20% state of charge and increased subsequently, the state of charge could not be determined from Fig. 2(a). The phase angle passed through a minimum as a function of frequency. The magnitude of the minimum decreased in the 0–20% state of charge range, and increased beyond 20% state of charge. The frequency at which the minimum occurred decreased with increase in state of charge from 20% to 80%.

The imaginary components of the impedance at various states of charge at fixed frequencies are presented in Tables 1 and 2 for Ni–Cd cells 1 and 3. (Since the ohmic resistance forms a substantial portion of the real component of impedance, it masks the real component of the electrode impedance. Hence only the imaginary component has been presented.) The imaginary component of the impedance (Z'') goes

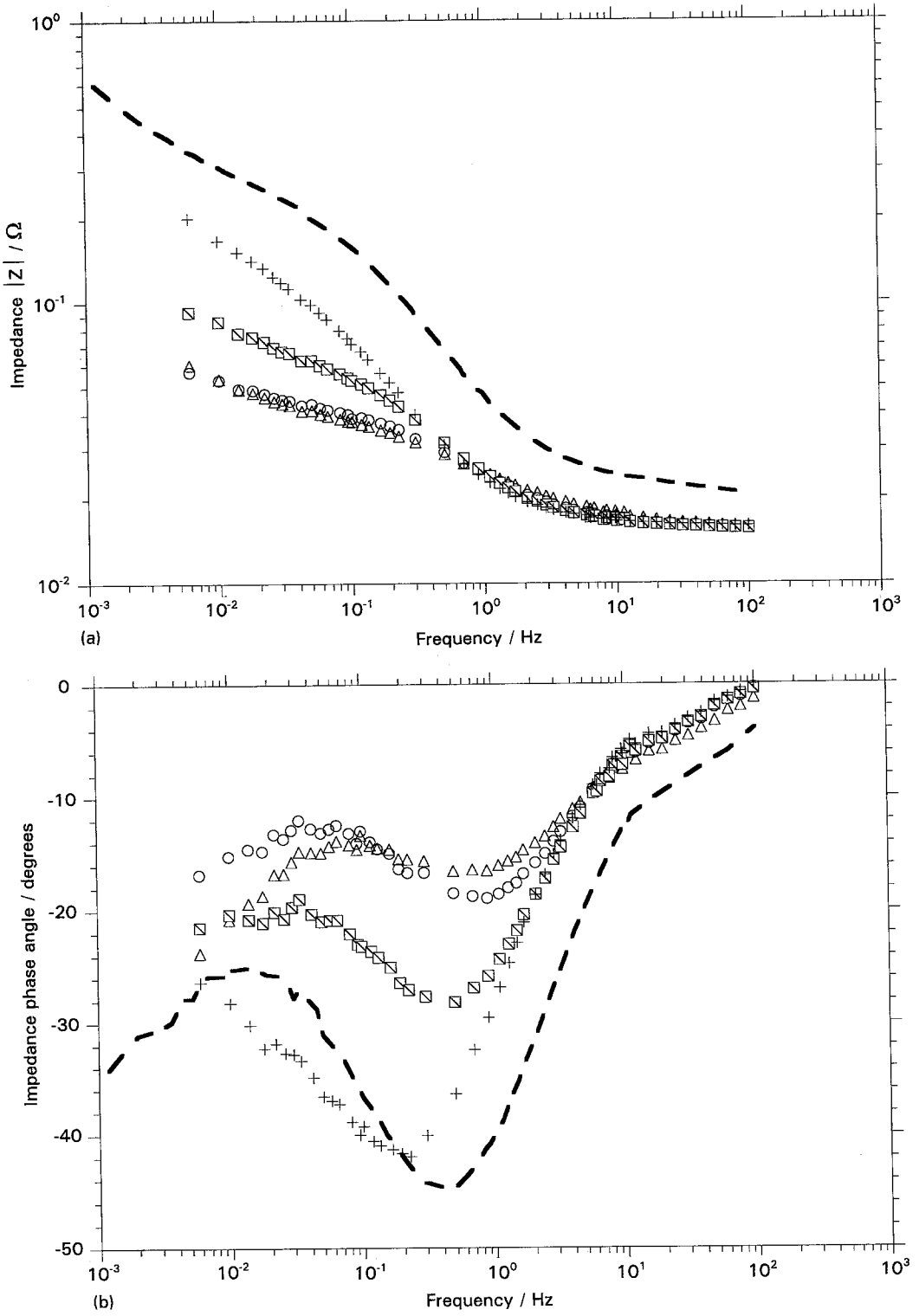

Fig. 2. Effect of state of charge on (a) magnitude of impedance $|Z|$, (b) impedance phase angle for Ni–Cd cell 5. Key: (— — —) 0%, (△) 20%, (○) 40%, (⊠) 60% and (+) 80%.

through a minimum for the cells in the frequency range tested. Hence the state of charge cannot be determined from the value of the imaginary component at a fixed frequency.

In light of the above problems, it was decided to use the approach of Sathyanarayana and Gopikanth [1, 13] and determine the effect of state of charge on ϕ, C_s and C_p at several frequencies, where C_s and C_p are the equivalent series and parallel capacitance, respectively, of the cell. Since impedance of batteries are very sensitive to state of charge at low frequencies, data was acquired at frequency as low as 0.006 Hz. Expressions for C_s and C_p are given below.

The battery impedance can be represented either as a series circuit R_sC_s or as a parallel circuit R_pC_p, where R_s and R_p are the equivalent series and parallel resistance, respectively. The imaginary component $-Z'' = 1/\omega C_s$. The following steps show the relationship between R_p and R_s and C_p and C_s.

The impedance of the battery Z is given by

$$Z = R_s - j/\omega C_s = (R_s\omega C_s - j)/\omega C_s \quad (1)$$

Table 1. Effect of state of charge on imaginary component (Z'') at various frequencies for Ni/Cd cell 1

	Imaginary component Z''/Ω				
SOC/(%)	*0.006 Hz*	*0.17 Hz*	*0.05 Hz*	*0.5 Hz*	*1.1 Hz*
0	0.206	0.0294	0.0543	0.0178	0.0123
10	0.0444	0.0126	0.0185	0.0120	0.011
20	0.0683	0.0188	0.0295	0.0146	0.011
40	0.0194	0.0079	0.0100	0.0066	0.0064
60	0.0316	0.0164	0.0190	0.0142	0.0127
80	0.0613	0.0603	0.0790	0.0347	0.0193
100	0.4938	0.0950	0.2220	0.0365	0.018

$$\frac{1}{Z} = \frac{\omega C_s(R_s C_s + j)}{(R_s\omega C_s - j)(R_s\omega C_s + j)} = \frac{R_s\omega^2 C_s^2}{1 + (R_s\omega C_s)^2} + \frac{j\omega C_s}{1 + (R_s\omega C_s)^2} \quad (2)$$

The impedance of the parallel R_pC_p circuit is given by

$$\frac{1}{Z} = \frac{1}{R_p} - \frac{\omega C_p}{j} \quad (3)$$

From Equations 2 and 3, the following relationships that express R_p and C_p in terms of R_s and C_s are obtained:

$$R_p = \frac{1 + (R_s\omega C_s)^2}{R_s\omega^2 C_s^2} \quad (4a)$$

$$C_p = \frac{C_s}{1 + (R_s\omega C_s)^2} \quad (4b)$$

Figures 3(a) and (b) show that ϕ and C_s are very sensitive to the state of charge at low frequencies. The phase angle passes through a minimum in Fig. 3(a) at all frequencies except at 25 Hz. C_s passes through a maximum in Fig. 3(b). Due to the greater sensitivity of the data with respect to state of charge at low frequency, the high frequency behaviour is not very clear from the above figures. Close examination of the data at each frequency showed that at certain frequencies, one of the above parameters increased or decreased with state of charge. Figure 4 shows that ϕ decreased with increase in state of charge at 25 Hz for Ni–Cd cells 5 and 6. Figure 5 shows that C_s increased with state of charge at 25 Hz for Ni–Cd cells 5 and 6, while C_p increased with SOC at 0.118 Hz and 0.226 Hz, as seen from Fig. 6. Hence the state of charge can be determined from Figs 4–6.

Table 2. Effect of state of charge on imaginary component (Z'') at various frequencies for Ni–Cd cell 3

	Imaginary component Z''/Ω					
SOC/(%)	*0.006 Hz*	*0.05 Hz*	*0.166 Hz*	*0.5 Hz*	*1.1 Hz*	*5.9 Hz*
0	0.3000	0.0926	0.0458	0.0226	0.0151	0.0068
20	0.0270	0.0136	0.0093	0.0070	0.0062	0.0039
40	0.0220	0.0134	0.0097	0.0067	0.0057	0.0030
60	0.0400	0.0255	0.0184	0.0132	0.0103	0.0042
80	0.0360	0.0374	0.0305	0.0345	0.0222	0.0066

Table 3. Inductive circuit parameter values for Ni–Cd cells 5 and 6 at 0% SOC

Ni–Cd Battery	*R/Ω*	*L/μH*
Cell 5	0.81	0.620
Cell 6	0.83	0.604

Although investigators have relied on impedance data at a fixed frequency to determine the state of charge of a battery, it is clear that such an approach may not always be successful. From the above results, it is evident that extensive tabulation of ϕ, C_s and C_p should be done at various states of charge at all frequencies. At certain frequencies, the above parameters pass through a maximum or minimum, thus making it difficult to determine the state of charge of the battery. At other frequencies, one or more of the above parameters increase or decrease with state of charge, thus enabling determination of SOC.

Separate criteria should be set for each cell type to determine the state of charge. These criteria are the dependence of ϕ, C_s or C_p on state of charge at a fixed frequency. The relevant plots for each cell should be obtained separately and used to determine its state of charge.

4.3. *Equivalent circuit results*

Figure 7 shows the modified Randles' circuit $R_\Omega(Q_1(R_tQ_2))$ to which the data was fitted. R_Ω is the ohmic resistance, Q_1 is the constant phase element representing double layer capacitance, R_t is the charge transfer resistance, and Q_2 is the constant phase element corresponding to the Warburg element. In some cases, the inductive portion was modelled by a parallel (RL) combination in series with the modified Randles' circuit. Table 3 gives the values of (RL) for Ni–Cd cells 5 and 6 at 0% state of charge. These parameters values were not determined for all states of charge, but the effect of state of charge on the inductance was determined qualitatively by noting the upper frequency limit for noninductive behaviour. The results are given in Table 4. This upper

Table 4. Upper frequency limit for noninductive behaviour for Ni–Cd cells

SOC/%	*Frequency (Hz) above which inductive behaviour is observed*			
	Cell 1	*Cell 3*	*Cell 5*	*Cell 6*
0	251	398	251	251
10	158.5			158.5
20	158.5	157.7	158	158.5
40	125	125.2	100	100
60	125.2	125.2	100	100
80	100	126	100	100
100	100	100	100	

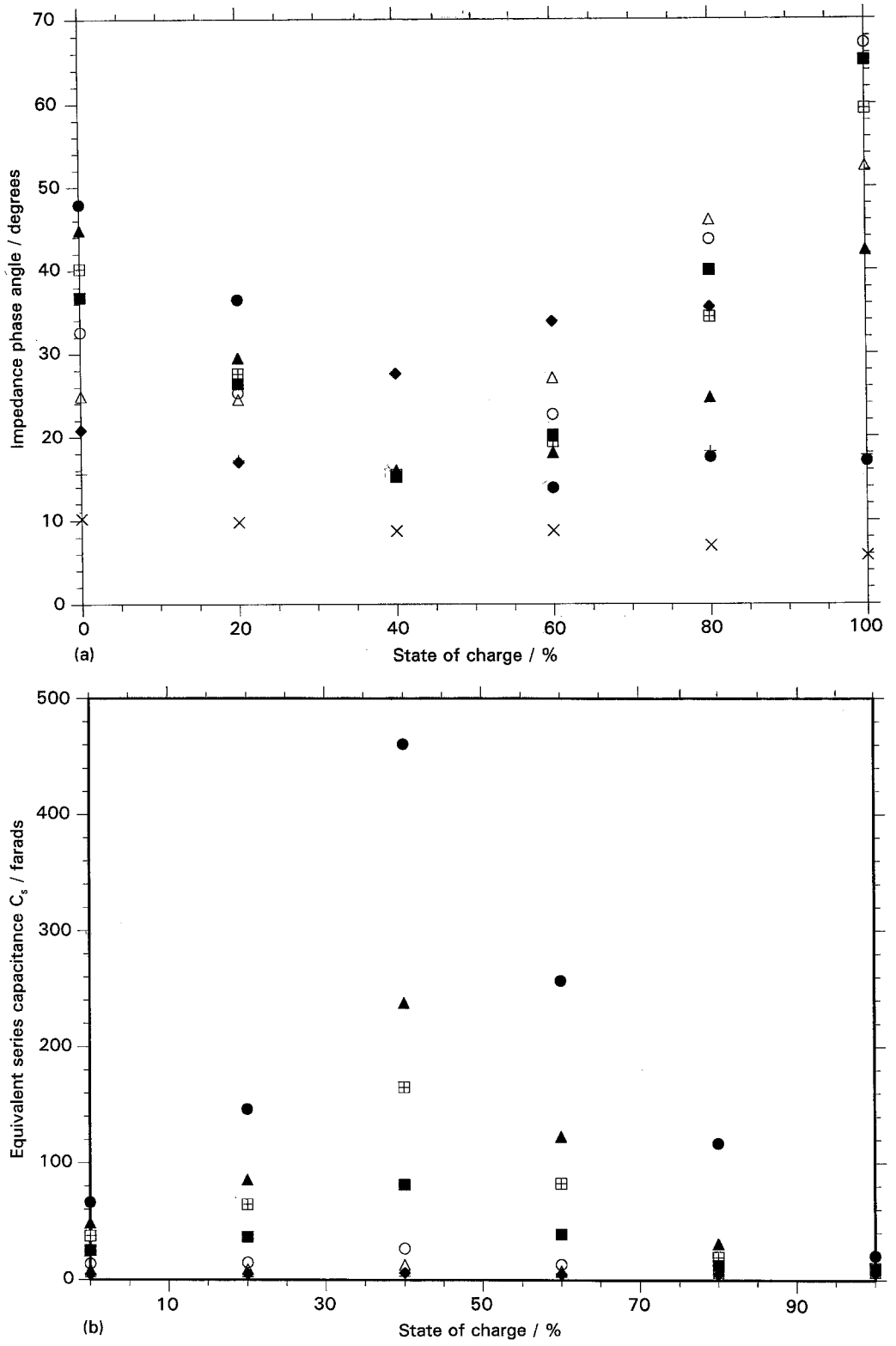

Fig. 3. Effect of state of charge on (a) impedance phase angle ϕ, (b) equivalent series capacitance C_s for Ni–Cd cell 1 at various frequencies.

Frequency/Hz	●	▲	⊞	■	○	△	◆	+	×
(a)	0.01	0.03	0.07	0.118	0.25	0.9	2.1	5.9	25.1
(b)	0.03	0.07	0.118	0.25	0.9	2.1	5.9	25.1	–

frequency limit decreased with increase in state of charge for each battery, showing a dependence of the inductive behaviour on state of charge.

The values of the circuit parameters with and without the inductive data are shown in Table 5. The (*RL*) values for the inductive portion have already been tabulated in Table 3. It is clear that fitting the data without the inductive points leads to nearly the same values for the circuit parameters as those obtained with the inductive points. Due to this, the inductive

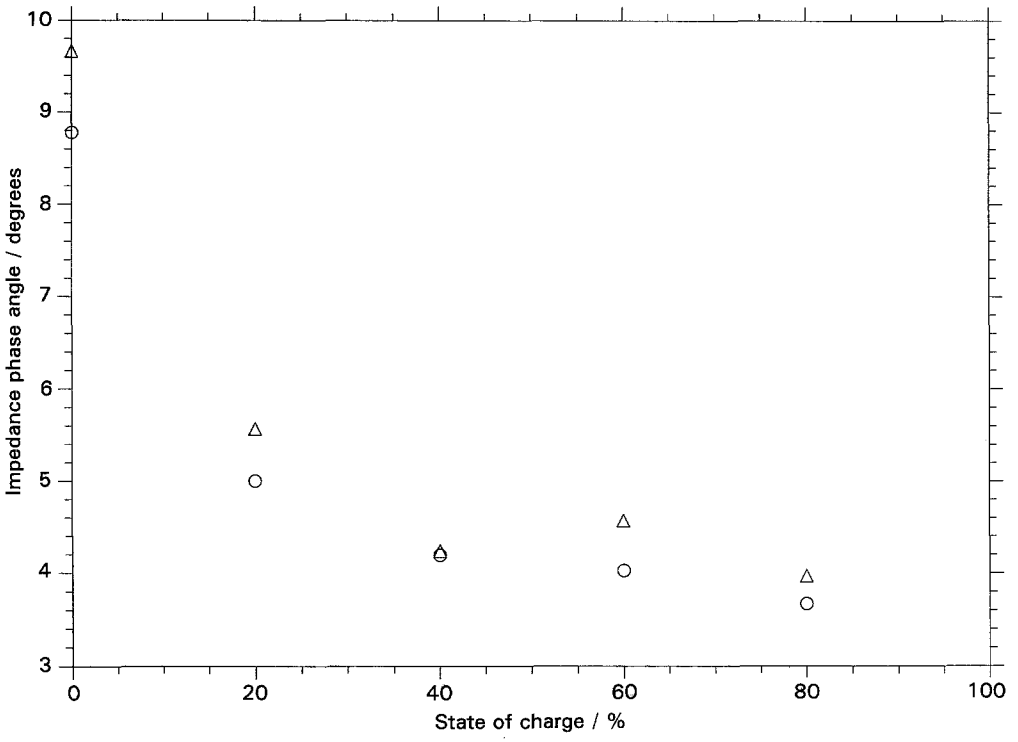

Fig. 4. Effect of state of charge on impedance phase angle ϕ at 25 Hz for Ni–Cd cell 5 (○) and cell 6 (△).

points in the data for all the cells were deleted prior to equivalent circuit fitting.

Figure 8 shows the Nyquist plot for Ni–Cd cell 5 at 60% state of charge. The semicircle is depressed at high frequencies. Tables 6–9 show the equivalent circuit parameter values for cells 1, 3, 5 and 6. Due to scatter in the data, reliable results at 100% SOC could not be obtained. For cells 1 and 3, the ohmic resistance decreased initially with increase in SOC, and then increased. The ohmic resistance decreased with increase in SOC for cells 5 and 6 in the 0–40% SOC range (Fig. 9). The charge transfer resistance R_t increased with state of charge. Figure 10 shows the increase in R_t with state of charge for cells 5 and 6 in the 20–80% SOC range. The R_t value at 0% was not plotted, since it was much higher than the value at other states of charge. Hence, plotting it obscured the effect in the 20–80% SOC range. This increase in R_t with state of charge may be due to depletion of charged active material, leading to

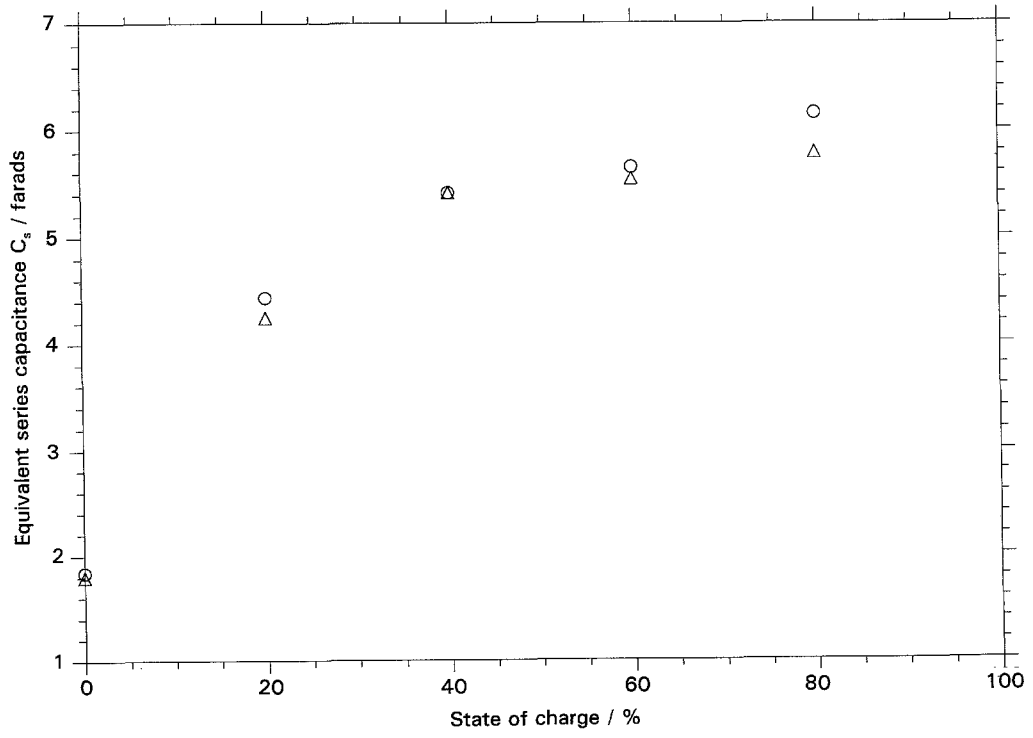

Fig. 5. Effect of state of charge on equivalent series capacitance C_s at 25 Hz for Ni–Cd cell 5 (○) and cell 6 (△).

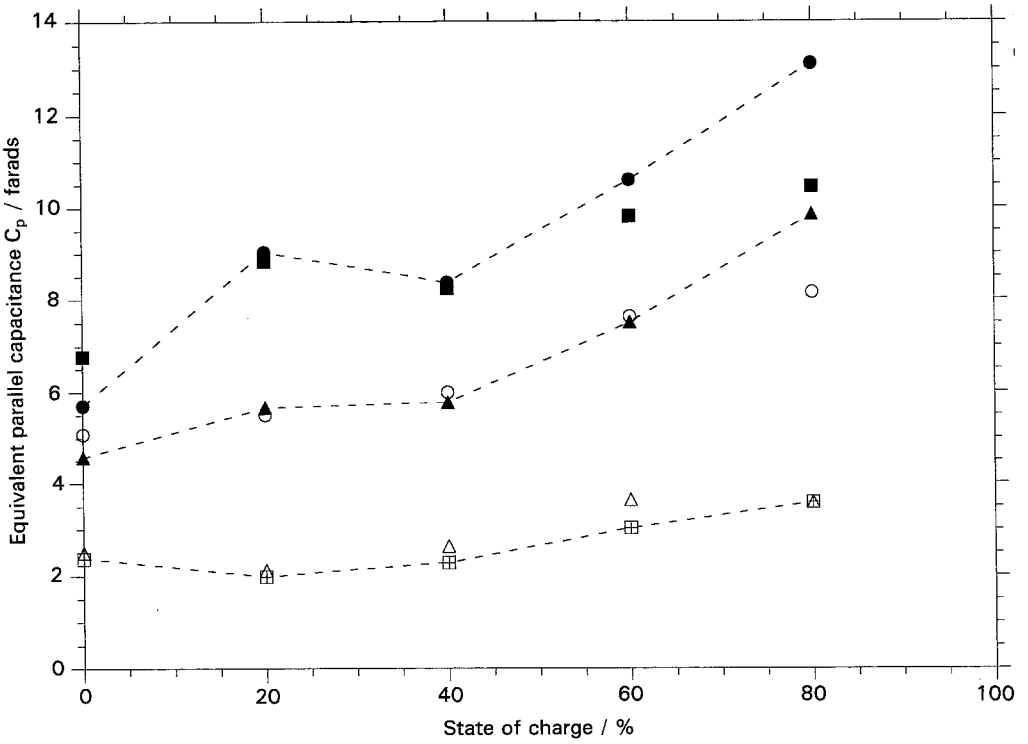

Fig. 6. Effect of state of charge on equivalent parallel capacitance C_p for Ni–Cd cells. Cell 5: (●) 0.118 Hz, (▲) 0.226 Hz and (⊞) 0.900 Hz; Cell 6: (■) 0.118 Hz, (○) 0.226 Hz and (△) 0.900 Hz.

Table 5. Effect of inductance on equivalent circuit parameter values

Nature of data	Ni–Cd battery	SOC/%	R_Ω/Ω	Y_1	n_1	R_t/Ω	Y_2	n_2
L*	cell 5	0	0.0200	6.60	0.780	0.240	32.3	0.530
			0.0210	6.45	0.800	0.200	30.0	0.520
L*	cell 6	0	0.0176	7.55	0.785	0.153	24.2	0.525
			0.0177	5.34	0.697	0.166	24.0	0.527

*L corresponds to fit with inductive points.

Table 6. Equivalent circuit parameters for Ni–Cd cell 1 for the circuit $R_\Omega(Q_1(R_tQ_2))$

SOC/%	$R_\Omega\Omega$	Y_1	n_1	R_t/Ω	Y_2	n_2
0	0.0136	15.6	0.526	0.0644	10.7	0.716
10	0.0100	9.57	0.570	0.0430	122.0	0.602
20	0.0121	16.3	0.572	0.0630	72.1	0.621
40	0.0117	8.37	0.768	0.0125	83.6	0.360
60	0.0113	9.78	0.754	0.0387	84.4	0.424
80	0.0132	8.70	0.850	0.156	213.8	0.675
100	0.0122	8.34	0.920	–	–	–

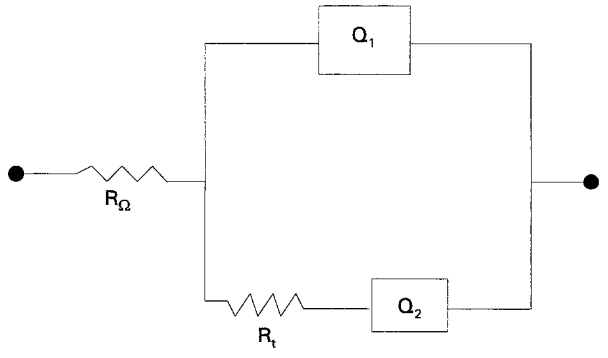

Fig. 7. Equivalence circuit used to fit impedance data.

Table 7. Equivalent circuit parameters for Ni–Cd cell 3 for the circuit $R_\Omega(Q_1(R_tQ_2)$

SOC/%	R_Ω/Ω	Y_1	n_1	R_t/Ω	Y_2	n_2
0	0.0158	2.8	0.700	0.009	15.0	0.553
20	0.0150	18.0	0.541	0.0263	100.4	0.460
40	0.0136	22.0	0.607	0.0207	75.7	0.335
60	0.0132	15.5	0.668	0.046	62.7	0.456
80	0.0139	7.0	0.795			
100	0.0144					

Table 8. Equivalent parameters for Ni–Cd cell 5 for the circuit $R_\Omega(Q_1(R_tQ_2)$

SOC/%	R_Ω/Ω	Y_1	n_1	R_t/Ω	Y_2	n_2
0	0.0220	6.5	0.812	0.228	35.0	0.558
20	0.0167	17.6	0.762	0.020	167.2	0.508
40	0.0157	17.1	0.768	0.025	219.5	0.484
60	0.0158	16.0	0.809	0.042	90.3	0.456
80	0.0164	16.9	0.845	0.089	29.9	0.413

Table 9. Equivalent circuit parameters for Ni–Cd cell 6 the circuit $R_\Omega(Q_1(R_tQ_2))$

SOC/%	R_Ω/Ω	Y_1	n_1	R_t/Ω	Y_2	n_2
0	0.0187	7.2	0.798	0.142	23.2	0.535
20	0.0146	15.2	0.732	0.021	193.5	0.514
40	0.0155	15.3	0.799	0.032	243.9	0.534
60	0.0145	13.9	0.839	0.053	106.1	0.422
80	0.0161	14.3	0.867	0.065	78.1	0.415

Table 10. Equivalent circuit parameters for the circuit $R_\Omega(Q_oR_o)(Q_1Q_2)$

Ni–Cd battery	*SOC /%*	R_Ω/Ω	Q_o Y_o	Q_o n_o	R_o/Ω	Q_1 Y_1	Q_1 n_1	R_t/Ω	Q_2 Y_2	Q_2 n_2
Cell 5	0	0.0200	2.38	0.952	0.0026	6.24	0.837	0.199	26.2	0.498
Cell 6	0	0.0164	1.70	1.00	0.0026	7.05	0.816	0.133	22.4	0.527

Table 11. Equivalent circuit parameters for the circuit $(R_\Omega Q_1(R_tO))$

Ni–Cd battery	*SOC/%*	R_Ω/Ω	Y_1	n_1	R_t/Ω	O Y_2	O B
Cell 3	60	0.0129	18.07	0.618	0.0627	94.2	8.10
Cell 5	80	0.0162	18.10	0.814	0.122	54.4	7.48

unavailability of active centres for charge transfer. The nonideal double layer capacitance Y_1 increased with state of charge between 0–20% SOC (Fig. 11).

At the fully discharged state, an additional high frequency arc was present for cells 5 and 6. Figure 12 shows the Nyquist representation for Ni–Cd cell 6 at 0% state of charge. Figure 13(a) shows the admittance representation for this data. The high frequency arc is very clear in this representation. This shows the usefulness of using different representations to identify arcs which may not be easily detected otherwise. Use of the modified Randles' circuit did not yield a good fit in the high frequency region. The use of a parallel (R_oQ_o) element in series with the modified Randles' circuit removed the high frequency error (Fig. 13(B)). Table 10 gives the equivalent circuit values for this fit. The high frequency points were deleted and the data was fitted with the modified Randles' circuit (Tables 8 and 9). If the high frequency arc is spurious, one cannot expect a good agreement between the remaining circuit parameters for the two circuits $R_\Omega(Q_1(R_tQ_2))$ and $R_\Omega(R_oQ_o)$ $(Q_1(R_tQ_2))$, i.e. (R_1, Q_1, R_t, Q_2). There is a good agreement between the above parameters for the two circuits as can be verified from Tables 8, 9 and 10. This additional arc was not observed at higher states of charge.

All the cases discussed so far yielded a nonideal Warburg diffusion element Q_2 in the low frequency region. Figure 14 shows that the low frequency data curves towards the real axis. This was modelled by a finite length diffusion element O. Table 11 gives the value of the circuit parameters for the data in which the finite diffusion element was used. To test the validity of this fit, the lowest frequency points that correspond to finite length diffusion were deleted and the data was fitted with the modified Randles' circuit. The

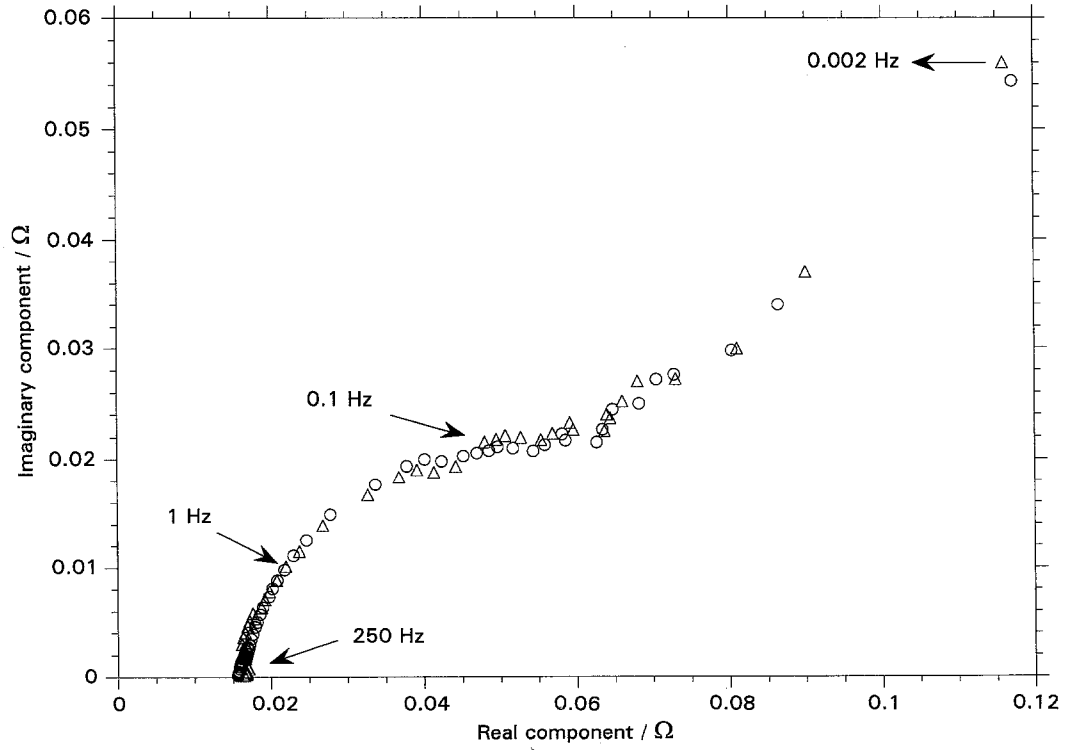

Fig. 8. Experimental (○) and calculated (△) impedance spectra for Ni–Cd cell 5 at 60% state of charge in the frequency range 0.002–100 Hz. (a) Nyquist plot; (b) Bode plot.

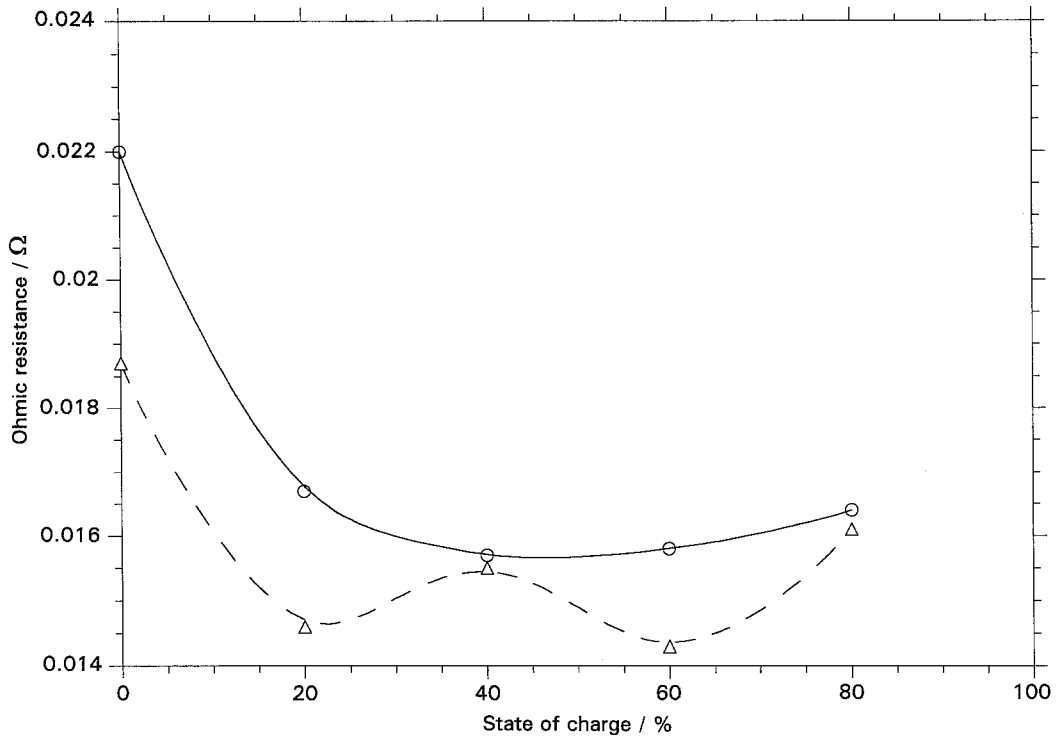

Fig. 9. Effect of state of charge on ohmic resistance R_Ω for Ni–Cd cell 5 (○) and cell 6 (△).

only difference between the modified Randles' circuit and the circuit with the finite diffusion element is the substitution of the CPE Q_2 with the finite diffusion element O. The values of the circuit parameters other than for O and Q_2) were quite close to each other. This can be confirmed by cross-checking the values of the circuit parameters from Tables 7 and 8.

5. Conclusions

Alternating current impedance measurements were obtained on sealed nickel cadmium cells. The dependence of state of charge on ϕ, C_s and C_p was determined. A modified Randles' equivalent circuit using constant phase elements to represent the

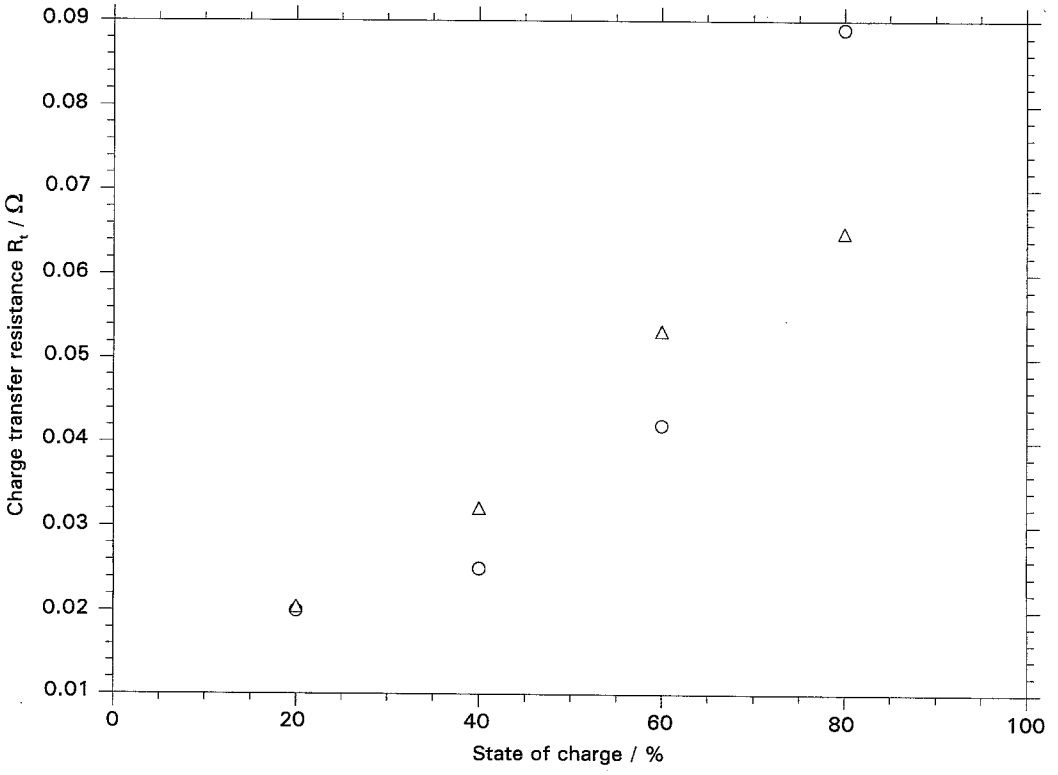

Fig. 10. Effect of state of charge on charge transfer resistance R_t for Ni–Cd cell 5 (○) and cell 6 (△).

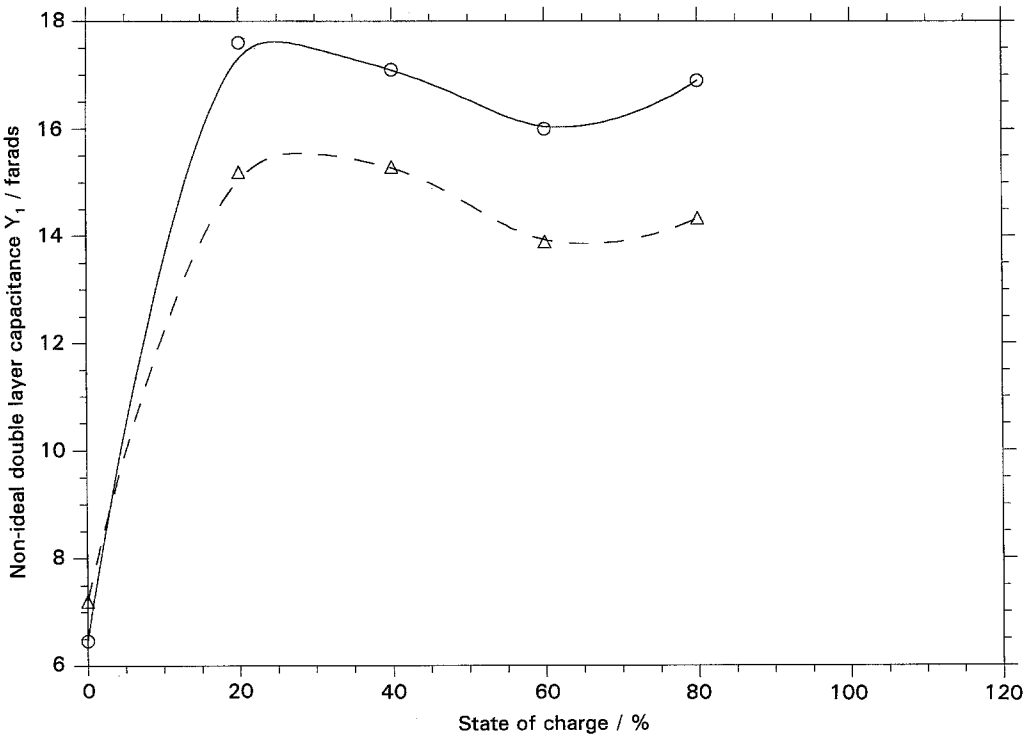

Fig. 11. Effect of state of charge on Y_1, the nonideal double layer capacitance for Ni–Cd cell 5 (○) and cell 6 (△).

double layer and Warburg impedance was used and the data was fitted to the circuit. The dependence of the state of charge on the circuit parameters was determined. A parallel (R_oQ_o) circuit was used in series with the rest of the circuit to fit the high frequency arc in the Nyquist plot. A finite diffusion element O was used to fit the low frequency data points bending over towards the real axis.

The following conclusions were drawn:

(i) A plot of the imaginary component as a function of state of charge at various frequencies gave rise to a minimum. Hence, the state of charge could not be determined from such plots.

(ii) The parameters ϕ, C_s and C_p were very sensitive to the state of charge at low frequency ($\sim$ 0.006–0.9 Hz).

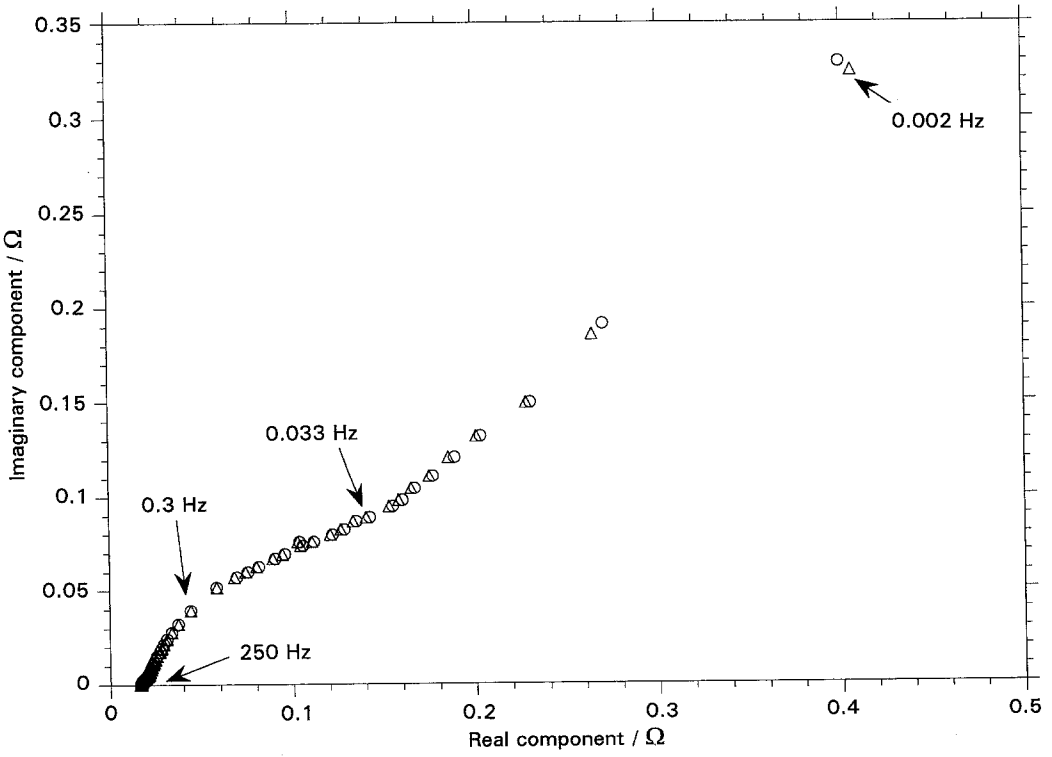

Fig. 12. Experimental (△) and calculated (○) impedance spectra (Nyquist plot) for Ni–Cd cell 6 at 0% SOC in the frequency range 0.002–251 Hz.

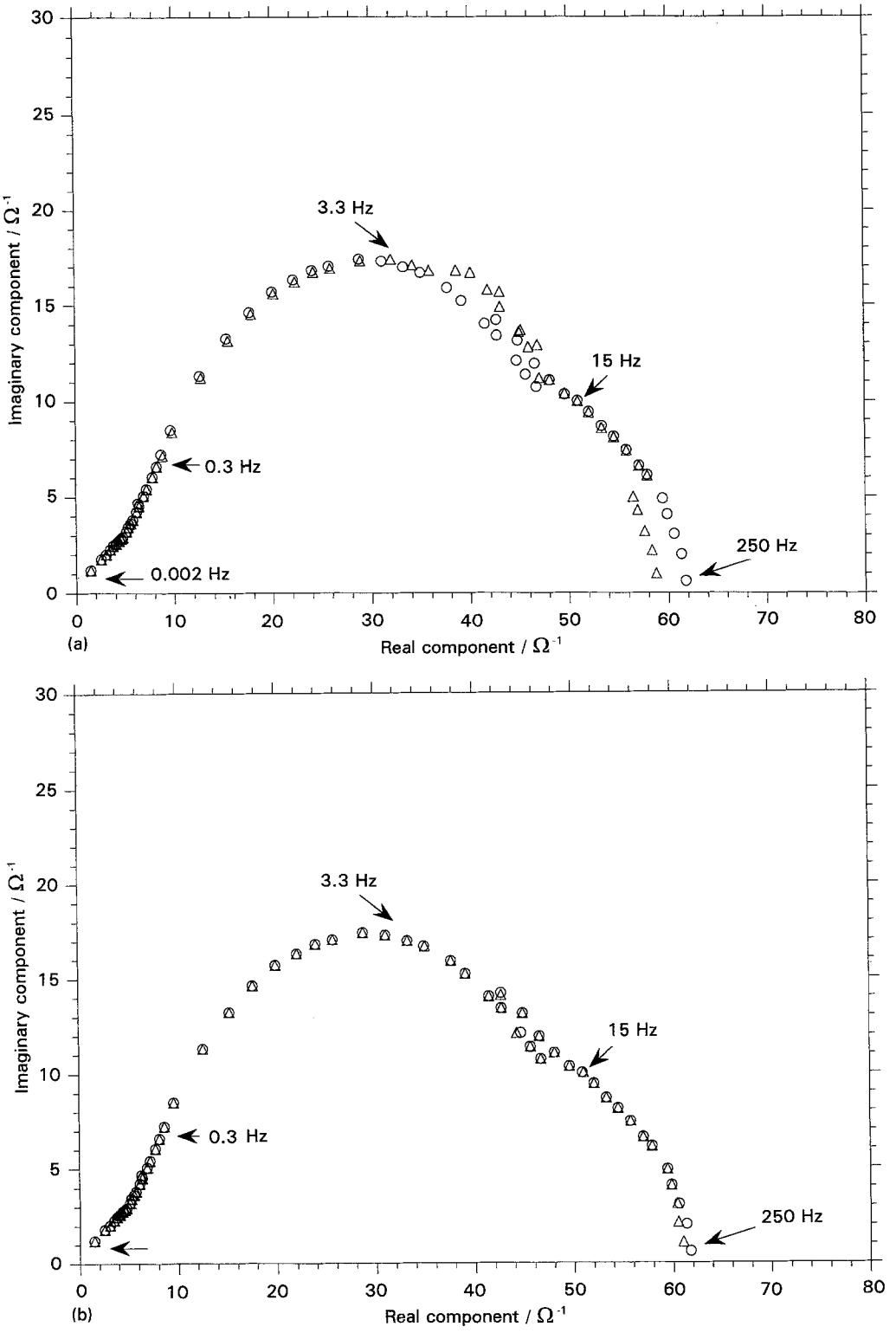

Fig. 13. Experimental (△) and calculated (○) impedance spectra (admittance plot) for Ni–Cd cell 6 at 0% state of charge in the frequency range 0.002–251 Hz. The equivalent circuits used were (a) $R(Q(RQ))$; (b) $R(RQ)(Q(RQ))$.

(iii) A complete tabulation of the above parameters at various frequencies as a function of the state of charge enabled the determination of the state of charge of the cell, since a monotonically increasing or decreasing relationship was obtained at certain frequencies.

(iv) A modified Randles' circuit with constant phase elements fit the data well. An additional arc at high frequency was modelled by a parallel (R_oQ_o) element in series with the rest of the circuit. The validity of this approach was confirmed by deleting the high frequency points and fitting with the modified Randles' circuit.

(v) The following results were obtained from the equivalent circuit analysis: (a) the ohmic resistance decreased with increase in state of charge, especially in the 0–20% SOC range; (b) the charge transfer resistance decreased in the 0–20% range, and

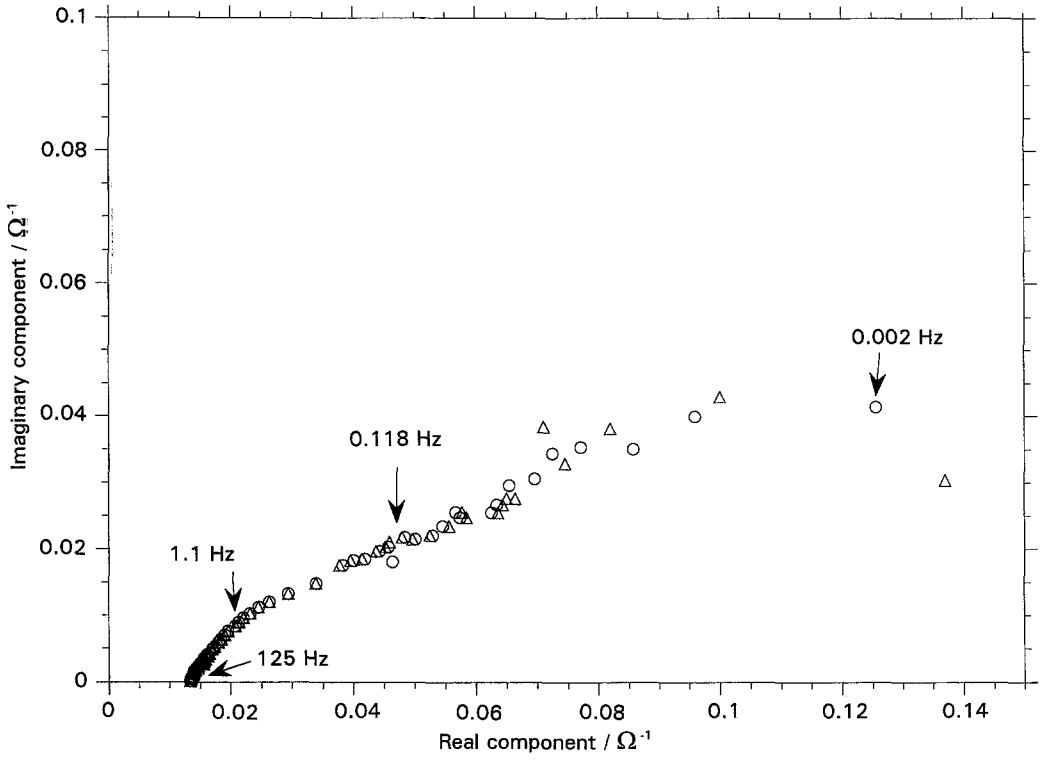

Fig. 14. Nyquist plot for finite diffusion at low frequency for Ni–Cd cell 3 at 60% state of charge. Fitting was done by using a finite diffusion element *O* instead of the Warburg element. (○) measurement; (△) simulation.

increased in the 20–80% SOC range; and (c) the nonideal double layer capacitance increased with increase in state of charge in the 0–20% SOC range.

References

[1] S. Sathyanarayana, S. Venugopalan and M. L. Gopikanth, *J. Appl. Electrochem.* **9** (1979) 125.
[2] R. T. Barton, M. Hughes, S. A. G. Karunathilaka and N. A. Hampson, *ibid.* **15** (1985) 399.
[3] M.S. Suresh and S. Sathyanaryana, *J. Power Sources* **37** (1992) 335.
[4] Ph. Blanchard, *J. Appl. Electrochem. 22* (1992) 1121.
[5] R. Haak, C. Ogden, D. Tench and S. Di Stefano, *J. Power Sources* **12** (1984) 289.
[6] M. A. Reid, *NASA Technical Memorandum 106105* (July 1992).
[7] M. A. Reid, *J. Power Sources* **29** (1990) 467.
[8] A. H. Zimmerman, M. R. Martinelli, M. C. Janecki and C. C. Badcock, *J. Electrochem. Soc.* **129** (1982) 289.
[9] EG&G PARC, Application note AC-1 (1989).
[10] C. Gabrielli, F. Huet, M. Keddam and J. F. Lizee, *J. Electroanal. Chem.* **138** (1982) 201.
[11] B. A. Boukamp, 'Equivalent Circuit Users Manual', 2nd edn, report: CT88/265/128, University of Twente, The Netherlands (May 1989).
[12] R. de Levie, *Electrochim. Acta* **8** (1963) 751.
[13] M. L. Gopikanth and S. Sathyanarayana, *J. Appl. Electrochem.* **9** (1979) 369.